Electrical, Surface Morphology and Magneto-Capacitance Properties of Pb Free Multiferroic $(BiFeO_3)_{1-x}(BaTiO_3)_x$ Solid Solutions

M. Shariq[a,b], D. Kaur[c], V.S. Chandel[a,*] and M.A. Siddiqui[a]

[a]Department of Physics, Integral University, Lucknow-226026, UP, India

[b]Department of Physics, Preparatory Year, Jazan University, Jazan-114, Saudi Arabia

[c]Functional Nanomaterials Research Laboratory, Department of Physics and Centre of Nanotechnology, Indian Institute of Technology, Roorkee 247667, India

(Received August 4, 2014; revised version March 22, 2015; in final form March 25, 2015)

The solid solutions $(BiFeO_3)_{1-x}(BaTiO_3)_x$ ($x = 0$, 0.1, 0.2, 0.3, 0.4, and 0.5) have been synthesized adopting a solid state sintering route. Well crystalline phase of $(BiFeO_3)_{1-x}(BaTiO_3)_x$ ceramics at different level of x has been optimized at sintering temperature of 950 °C for 2 h. Dielectric, polarization and magnetocapacitance properties were investigated for different content level of $BaTiO_3$. Dielectric constant increased with increasing concentration of $BaTiO_3$ up to $x = 0.3$ for all the frequencies of 10, 100, and 1000 kHz. Dielectric loss in the material is attributed to space charges, interfacial and dipolar polarizations. Measurements of P–E loop indicated evident ferroelectricity in all samples. Well formed grain with varying grain sizes and nearly uniform shape was found for ceramics samples.

DOI: 10.12693/APhysPolA.127.1675

PACS: 78.20.Ci, 81.05.Je, 81.40.Rs, 68.37.Yz

1. Introduction

Magnetoelectric (ME) multiferroics have attracted much attention for both fundamental physics and applied physics due to their unique coupling behavior between ferroelectricity, ferromagnetism, and ferroelasticity [1–3]. The coexistence of these ferroic orderings provides an additional degree of freedom especially useful for memory and logic device applications [4]. They not only can be used in ferroelectric and magnetic devices but also provide an additional degree of freedom in device design and applications, such as in the emerging field of spintronics [5], multiple state memory elements, electric field controlled ferromagnetic resonance devices and transducers with magnetically modulated piezoelectricity [6, 7]. $BiFeO_3$ (BFO) is the most important multiferroic material because it exhibits both G-type antiferromagnetism ($T_N \approx 640$ K) with a spatially modulated spin structure and ferroelectric ($T_C \approx 1100$ K) ordering at room temperature [8]. Multiferroic $BiFeO_3$ ceramic with a rhombohedrally distorted perovskite structure is a commensurate ferroelectric and an incommensurate antiferromagnet at room temperature [9].

Unfortunately, $BiFeO_3$ has poor ferroelectric performance due to severe electric leakage both in thin films and in bulks. It is believed that the electrical leakage is caused by oxygen vacancies and iron ions with different valences via the formation of shallow energy centers [10]. $BiFeO_3$ presents some drawback, too, especially in bulk form such as spiral spin modulation, weak magnetoelectric effect, and low resistivity which has prevented practical application of the material as piezoelectric or magnetoelectric functional components.

Different kind of chemical modifications have been performed in the improvement of multiferroic properties of $BiFeO_3$. At present, two ways are used to solve the problem, one is to process $BiFeO_3$ with other perovskite structured materials (such as $PbTiO_3$, $BaTiO_3$, and $SrTiO_3$) [11–13] into solid solution in order to prevent the formation of secondary phases and enhance the electrical insulation resistivity, the other is to add some dopants such as lanthanum [14], gallium [11], and neodymium [15]. $BaTiO_3$ (BTO) appears to be one of the most promising end materials because the introduction of $BaTiO_3$ not only stabilizes the perovskite phase but also forms a morphotropic phase boundary. In addition, $BaTiO_3$ is Pb free material and Ti substitution at the Fe sites can increase the magnetization of the novel compounds [16]. In present work, multiferroic $(BiFeO_3)_{1-x}(BaTiO_3)_x$ (BF–BT) solid solutions were synthesized by solid state reaction route. Dense BF–BT ceramics were processed and their micro structural, ferroelectric, magnetocapacitance and dielectric properties were carefully investigated.

2. Experimental details

$BiFeO_3$ ceramic was prepared from Bi_2O_3 and Fe_2O_3 as reactants by solid state reaction method followed by calcination at the 600 °C for 2 h and sintering at temperature of 870 °C for 5 min. In order to avoid an im-

*corresponding author; e-mail: chandel.integral@gmail.com

purity phase of $Bi_2Fe_4O_9$ and unreacted Bi_2O_3 during synthesis process, an excess amount of Bi_2O_3 (10% extra on weight basis) was added to the starting reactants. $BaTiO_3$ was prepared by the solid state route using materials of commercial reagent-grades of TiO_2 and $BaCO_3$ with purity ≈99.8%. These reactants were carefully weighed in stoichiometric proportions (1:1 mole ratio) and mixed thoroughly by grinding in an agate mortar. Mixed powder was calcinated in furnace for 2 h at the temperature of 800 °C then followed by sintering at temperature of 950 °C to achieve perovskite phase formation of $BaTiO_3$. Now, $BiFeO_3$ and $BaTiO_3$ were mixed in stoichiometric amounts and grinded for 4 h in agate mortar followed by calcination at the temperature of 800 °C for 2 h. Samples of different composition were mixed with a few drops of 6% concentrated aqueous polyvinyl alcohol (PVA) binder and again grinded in the agate mortar for 2 h. Mixed powders with different composition were pressed into pellets with a pressure of 1.47×10^8 Pa. In order to evaporate aqueous polyvinyl alcohol, these pellets of different compositions were heated subsequently at temperature of 250 °C for 1 h. These pellet of $(BiFeO_3)_{1-x}(BaTiO_3)_x$ with different compositions were sintered at 950 °C for 2 h. The samples are named after their compositions, e.g., 90BF-10BT stands for $(BiFeO_3)_{0.9}(BaTiO_3)_{0.1}$.

P–E hysteresis loops of $(BiFeO_3)_{1-x}(BaTiO_3)_x$ were measured using precision PremierII (Radiant technology) ferroelectric tester. Dielectric and magnetocapacitance were measured by computer controlled LCR meter. Field emission scanning electron microscope (FEI Quanta 200F model) was used to study the surface morphology of different samples. Energy dispersive X-ray analysis was carried out to confirm the concentrations and ratio of elements Bi, Fe, O, Ba, and Ti in $(BiFeO_3)_{1-x}(BaTiO_3)_x$ ceramics.

3. Results and discussion

The dielectric constant is represented by $\varepsilon = \varepsilon' - \varepsilon''$, where ε' is real part of dielectric constant (relative permittivity) and describes the stored energy while ε'' is imaginary part of dielectric constant, which describes the dissipated energy.

Figure 1 shows the variation of dielectric constant (ε_r) of $(BiFeO_3)_{1-x}(BaTiO_3)_x$ as a function of frequency at room temperature for $x = 0$, 0.1, 0.2, 0.3, 0.4, and 0.5, respectively. The dielectric constant for all the samples decreases with increasing frequency, as can be expected from a conventional dielectric relaxation process. This is very much consistent with a normal behavior of a dielectric. At lower frequency, ε' is expected to be higher due to the presence of all the different types of polarizations (i.e., interface, dipole, ionic, atomic, electronic, etc.). The value of the dielectric constant of $BiFeO_3$ agrees well with that reported by Mahesh et al. [17] and Singh et al. [18]. However, the dip at 10^5 kHz observed in the frequency dependence of dielectric constant of $BiFeO_3$ is absent in our data; for all the samples investigated, a smooth curve has been obtained (Fig. 1).

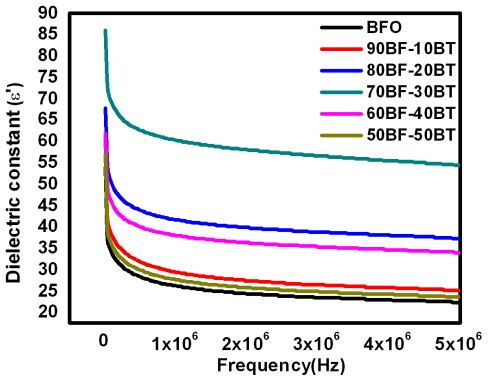

Fig. 1. Frequency dependence of dielectric constant (ε') of BF-BT system for $x = 0$, 0.1, 0.2, 0.3, 0.4 and 0.5 at room temperature.

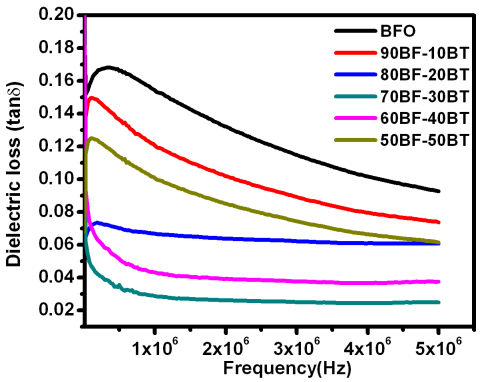

Fig. 2. Frequency dependence of dielectric loss ($\tan\delta$) of BF-BT system for $x = 0$, 0.1, 0.2, 0.3, 0.4 and 0.5 at room temperature.

Figure 2 shows the frequency dependence of dielectric loss in BF–BT ceramics. The dielectric loss $\varepsilon''(\tan\delta)$ also decreases smoothly with increasing frequency. Dielectric loss is found to increase with frequency up to 500 kHz then decreases slowly at higher frequency. Dielectric loss arises if the polarization lags behind the applied alternating field and polarization lag is caused by the presence of the impurities and structural non-homogeneities. The decrease in $\tan\delta$ with increase in frequency is in accordance with the Koops phenomenological model [19]. Dielectric loss ε'' is also found to decrease with increasing the content of $BaTiO_3$ in BF–BT ceramics, justifying enhancement in resistivity with incorporation of $BaTiO_3$.

To investigate further the effect of $BaTiO_3$ substitution, the dielectric constant and dielectric loss of the $(BiFeO_3)_{1-x}(BaTiO_3)_x$ ceramics are re-plotted as a function of content of $BaTiO_3$ (Fig. 3). It is striking to see that dielectric constant increases with increasing content of $BaTiO_3$ up to $x = 0.3$ for all the frequency of 10, 100, and 1000 kHz (Fig. 3a). Further increase of content of $BaTiO_3$ (after $x = 0.3$) reduces the value of dielectric constant.

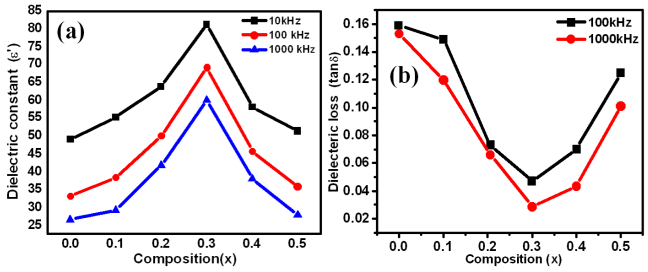

Fig. 3. Variation of dielectric constant (a) and loss ($\tan\delta$, (b)) with x for $(BiFeO_3)_{1-x}(BaTiO_3)_x$ system.

This dielectric behavior of $(BiFeO_3)_{1-x}(BaTiO_3)_x$ ceramics might be understood in terms of oxygen vacancy and the displacement of Fe^{3+} ions. There are always some oxygen vacancies in pure $BiFeO_3$, which results in relatively high conductivity and small dielectric constant. Substitution of Bi for Ba and Fe for Ti would stabilize the perovskite structure of $BiFeO_3$ and hence reduce the number of oxygen vacancies and subsequently increases the dielectric constant. Also on the other hand, for $BaTiO_3$ content $x \leq 0.3$, the mismatch between $BiFeO_3$ and $BaTiO_3$ lattice constant prevents the grains from growing big, which introduces more grain boundaries. As a result, the resistivity and the dielectric constant would increase again. Further increase in $BaTiO_3$ content ($x > 0.3$) would result in a unit cell volume contraction because ionic radius of Ba is smaller than that of Bi. The free volume available for the displacement of Fe^{3+} ions in the Fe–O oxygen octahedral becomes smaller and this would lead to a decrease in dielectric polarization. Figure 3b shows variation of dielectric loss with composition x. Minimum tangent loss and maximum dielectric constant occur at $x = 0.3$ for all frequencies. In general, it is believed that the dielectric loss is due to a space charges and interfacial and dipolar polarizations [20]. Dielectric relaxation due to a space charge or interfacial polarization occurs at low frequency. The abundant space charges are suggested as originating from the aliovalent substitutions of Ba^{2+} and Ti^{4+}.

Figure 4a–e shows the P–E hysteresis curves of BF–BT ceramics at room temperature. Measurements were performed at a frequency of 1 Hz. Figure 4 indicates that all samples exhibit evident ferroelectricity. The coercive electric field increases at first: become maximum for $x = 0.2$ and then decreases, being minimum at $x = 0.3$ then again increases with increasing content of $BaTiO_3$. Table shows values the coercive electric field, remnant polarization, and saturation polarization of samples at $x = 0$, 0.1, 0.2, 0.3, and 0.4.

It has been reported that remnant polarization (P_r) and coercive field (E_c) values of perovskite-type ferroelectric material are affected by various factors, such as the displacement of polar ions [21], domain pinning by defects [22] and orientation [23], etc. In this study, enhanced values of Pr seems due to Ba^{2+} ions replacing Bi^{3+} ions in the perovskite unit cell, releasing the

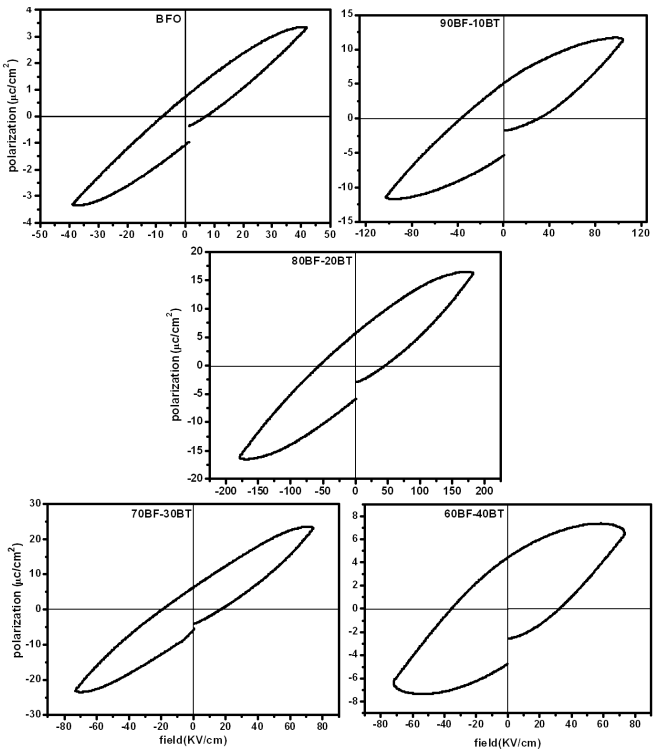

Fig. 4. Ferroelectric P–E loops for BF–BF system (a) $x = 0$, (b) $x = 0.1$, (c) $x = 0.2$, (d) $x = 0.3$, (e) $x = 0.4$.

TABLE

Various polarization parameter of BF–BT system.

Composition (x)	Coercive field [kV/cm]	Remnant polarization [μC/cm^2]	Saturation polarization [μC/cm^2]
0	7.8	0.73	03.37
0.1	37.4	5.25	11.78
0.2	56.5	5.72	16.47
0.3	19.2	6.41	23.70
0.4	35.2	4.52	–

dislocation of the Fe^{3+} ion in the (111) direction (this dislocation originated from Bi–O orbital hybridization [24], resulting in a destruction of the cycloid order of the $BiFeO_3$ structure ($R3c$). In fact, the hybridization of Ti–O orbitals supports the dislocation of the Ti^{4+} ion in the (100) direction. In addition, hysteresis loop BFO slightly shift to the positive bias field, which could be attributed to crystallographic defect distribution, and thermal history between top electrode and bottom electrodes [25]. P–E loops can attain saturation indicating that the doped specimens can be poled fully whereas P–E loop of the sample with $x = 0.4$ shows round corners, indicating significant conductive losses (Fig. 4). The leakage current is reduced with content of $BaTiO_3$, being minimum for 70BF–30BT, indicating highest resistivity at this composition. The structure of the specimen for $x = 0.3$ belongs to morphotropic phase boundary (MPB), providing

better polarization properties. The sintering ability of the undoped sample is poor and the grain size is inhomogeneous, which is not beneficial for domains reversal. Sintering property was improved at $x = 0.3$ with homogeneous grain size, which is beneficial for domains reversal, therefore the coercive field of $(BiFeO_3)_{1-x}(BaTiO_3)_x$ is low at $x = 0.3$. However, with further increase in the content of $BaTiO_3$, the coercive electric field increases due to creation of oxygen vacancies. The appearance of the oxygen vacancies will lead to oxygen octahedral distortion, resulting in a pinning effect on domains reversal. Therefore, the coercive field increases, making the materials "hard".

Figure 5 shows the magnetic field dependence of dielectric constant of BF–BT solid solutions. Dielectric constant changes with magnetic field for all the composition and change is appreciable for $x = 0.1$, 0.2 and approximately constant for $x = 0.3$, 0.4.

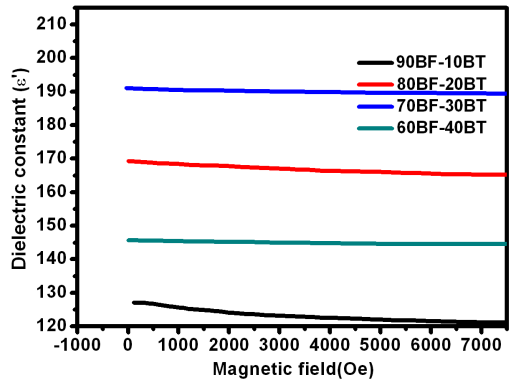

Fig. 5. Variation of dielectric constant with magnetic field at room temperature.

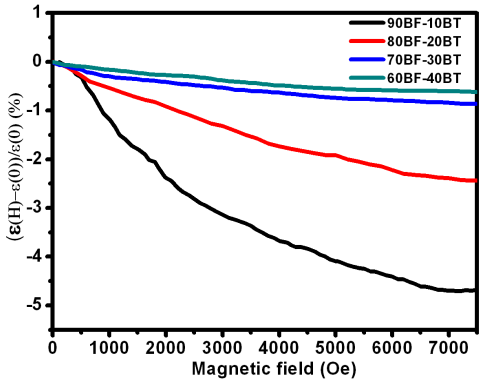

Fig. 6. Variation of magnetocapacitance with magnetic field at room temperature.

Figure 6 shows the variation of magnetocapacitance (MC) with applied magnetic field. Magnetoelectric capacitance is defined by the equation:

$$\mathrm{MC} = \frac{\varepsilon(H) - \varepsilon(0)}{\varepsilon(0)} \times 100, \qquad (1)$$

where $\varepsilon(H)$ and $\varepsilon(0)$ are dielectric constant in presence of magnetic and in absence of magnetic field. Magnetocapacitance decreases with magnetic field and shows negative values. All compositions of $(BiFeO_3)_{1-x}(BaTiO_3)_x$ solid solutions have negative magnetocapacitance similarly like most ferromagnetic and antiferromagnetic materials and show a decrease in dielectric constant and capacitance. The variation of MC at $x = 0.1$ and 0.2 is much appreciable because of strong coupling due to ferromagnetic nature of BF–BT system up to $x = 0.2$. The variation of dielectric constant and magnetocapacitance for 70BF–30BT and 60BF–40BT are not much significant because of weak coupling due to paramagnetic nature of these compositions.

Field emission scanning electron microscope (FE-SEM) is used to find topography (the surface features of an object) and morphology (the shape, size and arrangement of the particles making up the object that are lying on the surface of object). Figure 7 shows SEM images of $(BiFeO_3)_{1-x}(BaTiO_3)_x$ solid solutions for all different levels of x as 0, 0.1, 0.2, 0.3, 0.4 and 0.5, respectively. These images were taken from fresh fractured surfaces of different samples. High tendency of densification can be observed for different ceramic samples sintered at 950 °C. Well formed grain of sintered $(BiFeO_3)_{1-x}(BaTiO_3)_x$ ceramics with varying grain sizes and nearly uniform shape touching each other with somewhere free spaces lingering between them are shown in Fig. 7a–f. It revealed the average grain size of ceramic samples approximately 1–2 μ m. Large grains are probably related to the agglomeration and not to a particular sintering mechanism leading to abnormal grain growth. Formation of atomic defects due the content of $BaTiO_3$ could also play a role to change the grain size.

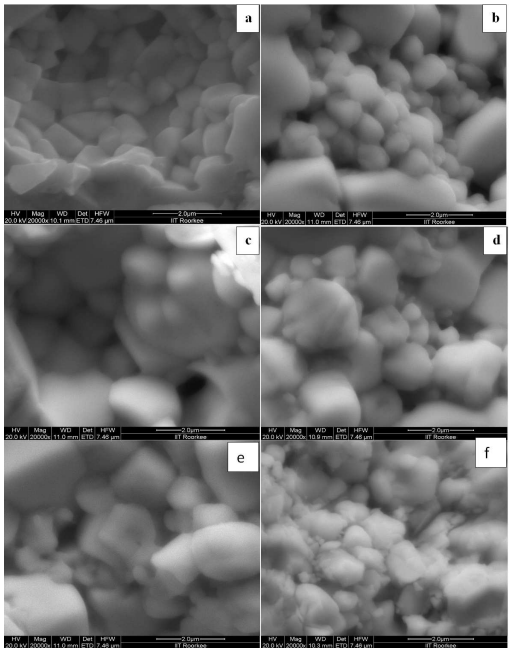

Fig. 7. Scanning electron micrographs for $(BiFeO_3)_{1-x}(BaTiO_3)_x$ solid solution with various composition (a) $x = 0$, (b) $x = 0.1$, (c) $x = 0.2$, (d) $x = 0.3$, (e) $x = 0.4$ and (f) $x = 0.5$.

The undoped sample i.e. $BiFeO_3$ shows small and inhomogeneous grain size, which results in significant residual porosity. The grain size of ceramic samples was increased with the content of $BaTiO_3$ up to $x = 0.3$ improving the sintering ability of solid solution accordingly. Whereas grain size of BF–BT ceramics decreases for $x > 0.3$ lowering the sintering ability of the BF–BT solid solution (Fig. 7). Ba, Ti ions will enter crystal lattices substituting Bi and Fe for $x \leq 0.3$, which will lead to crystal lattice distortion, improving the sintering ability of the ceramics. Content of $BaTiO_3$ above 0.4 ($x > 0.4$) may probably exceed the solubility limit of Ba, Ti ions in the solid solution, thus sintering ability of the ceramic and the properties of the material are deteriorated accordingly.

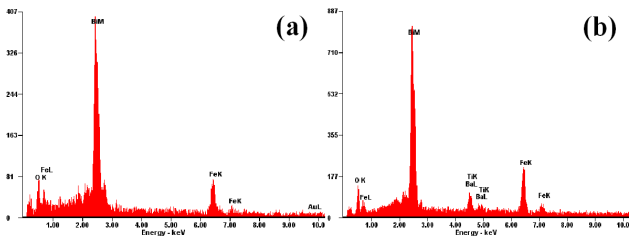

Fig. 8. EDAX spectrum of samples $BiFeO_3$ and $(BiFeO_3)_{0.9}(BaTiO_3)_{0.1}$ ceramics.

In order to check the expected atomic percentage (%) of different elements present in the ceramics, we introduced energy dispersive X-rays spectroscopy (EDXS) of two samples of $BiFeO_3$ and $(BiFeO_3)_{0.9}(BaTiO_3)_{0.1}$. Figure 8 shows the EDXS spectrum of two ceramic samples. Atomic percentage of Bi, Fe, Ba, Ti, O elements in samples of $BiFeO_3$ and $(BiFeO_3)_{0.9}(BaTiO_3)_{0.1}$ are obtained near to their expected values. Small peak of gold (Au) is observed in EDXS spectrum due to gold coating on the sample surface to make it conducting, required for FE-SEM. However; EDXS has not returned the exact expected results after allowing for errors within the EDXS system. This discrepancy can attributed to a variety of causes, such as the sample contamination by the flux and interference due to surface topography. Thus EDXS analysis also verified the chemically homogeneity of each element and relative ratio.

4. Conclusions

The dielectric constant for all the samples decreased with increasing frequency, as can be expected from a conventional dielectric relaxation process. Dielectric loss ε'' was also found to decrease with increase of the content of $BaTiO_3$ in BF–BT ceramics, justifying enhancement in resistivity with incorporation of $BaTiO_3$. Dielectric constant changed with magnetic field for different samples of $(BiFeO_3)_{1-x}(BaTiO_3)_x$ ceramics. All compositions of $(BiFeO_3)_{1-x}(BaTiO_3)_x$ solid solutions had negative magnetocapacitance similar like most ferromagnetic and antiferromagnetic materials and showed a decrement in dielectric constant and capacitance. Well formed grains of ceramics samples with varying grain size and nearly uniform shape touching each other with somewhere free spaces lingering between them were obtained.

References

[1] K.F. Wang, J.-M. Liu, Z.F. Ren, *Adv. Phys.* **58**, 321 (2009).

[2] C.W. Nan, M.I. Bichurin, S.X. Dong, D. Viehland, G. Srinivasan, *J. Appl. Phys.* **103**, 031101 (2008).

[3] W. Eerenstein, N.D. Mathur, J.F. Scott, *Nature London* **442**, 759 (2006).

[4] M. Bibes, A. Barthelemy, *Nature Mater.* **7**, 425 (2008).

[5] N. Hur, S. Park, P.A. Sharma, J.S. Ahn, S. Guha, S.W. Cheong, *Nature* **429**, 392 (2004).

[6] G. Catalan, H. Béa, S. Fusil, M. Bibes, P. Paruch, A. Barthélémy, J.F. Scott, *Phys. Rev. Lett.* **100**, 027602 (2008).

[7] M. Shariq, D. Kaur, V.S. Chandel, M.A. Siddique, *Mater. Sci. Poland* **31**, 471 (2013).

[8] C. Ostos, O. Raymond, N. Suarez-Almodovar, D. Bueno-Baque, L. Mestres, J.M. Siqueiros, *J. Appl. Phys.* **110**, 024114 (2011).

[9] P. Pandit, S. Satapathy, P.K. Gupta, *J. Appl. Phys.* **106**, 114105 (2009).

[10] X.D. Qi, J. Dho, R. Tomov, M. Blamire, J.L. Macmanus Driscoll, *Appl. Phys. Lett.* **86**, 062903 (2005).

[11] J.R. Cheng, N. Li, L. Eric Cross, *J. Appl. Phys.* **94**, 5153 (2003).

[12] M.M. Kumar, A. Srinivas, S.V. Suryanarayana, *J. Appl. Phys.* **87**, 855 (2000).

[13] T.L. Ivanova, V.V. Gagulin, *Ferroelectrics* **265**, 241 (2002).

[14] G. Le Bras, D. Colson, A. Forget, N. Genand-Riondet, R. Tourbot, P. Bonville, *Phys. Rev. B* **80**, 134417 (2009).

[15] V.L. Mathe, K.K. Patankar, R.N. Patil, C.D. Lokhande, *J. Magn. Magn. Mater.* **270**, 380 (2004).

[16] W.M. Zhu, Z.G. Ye, *Appl. Phys. Lett.* **89**, 232904 (2006).

[17] M.K. Mahesh, V.R. Palkar, K. Srinivasan, *Appl. Phys. Lett.* **76**, 2764 (2000).

[18] K. Singh, N.S. Negi, R.K. Kotnala, M. Singh, *Solid State Commun.* **148**, 18 (2008).

[19] C.G. Koops, *Phys. Rev.* **83**, 121 (1951).

[20] J. Wang, X.G. Tang, H.L.W. Chan, C.L. Choy, H. Luo, *Appl. Phys. Lett.* **86**, 152907 (2005).

[21] Y. Wu, G. Cao, *J. Mater. Sci. Lett.* **19,** 267 (2000).

[22] M. Grossmann, O. Lohse, D. Bolten, U. Boettger, T. Schneller, R. Waser, *J. Appl. Phys.* **92**, 2680 (2002).

[23] C.J. Lu, X.L. Liu, X.Q. Chen, C.J. Nie, G.L. Rhun, S. Senz, D. Hesse, *Appl. Phys. Lett.* **88**, 162905 (2006).

[24] M.M. Kumar, A. Srinivas, S.V. Suryanarayana, *J. Appl. Phys.* **87**, 855 (2000).

[25] Y.H. Lee, J.M. Wu, Y.L. Chueh, L.-J. Chou, *Appl. Phys. Lett.* **87**, 172901 (2005).